Vol 18 No 7, July 2009
1674-1056/2009/18(07)/2868-05

Chinese Physics B

© 2009 Chin. Phys. Soc.
and IOP Publishing Ltd

Application of sampled grating to control the lasing wavelength in complex-coupled DFB laser*

Wang Huan(王 桓)[a)†], Zhu Hong-Liang(朱洪亮)[a)], Jia Ling-Hui(贾凌慧)[b)], Chen Xiang-Fei(陈向飞)[b)], Kong Duan-Hua(孔端花)[a)], Wang Lie-Song(王列松)[a)], Zhang Wei(张 伟)[a)], Zhao Ling-Juan(赵玲娟)[a)], and Wang Wei(王 圩)[a)]

[a)] *Key Laboratory of Semiconductor Materials Science, Institute of Semiconductors, Chinese Academy of Sciences, Beijing* 100083, *China*

[b)] *Microwave-Photonics Technology Laboratory, Nanjing National Laboratory of Microstructures, Nanjing University, Nanjing* 210093, *China*

(Received 13 October 2008; revised manuscript received 30 October 2008)

This paper reports that the complex-coupled distributed feedback laser with the sampled grating has been designed and fabricated. The +1st order reflection of the sampled grating is utilized for laser single mode operation, which is 1.5387 μm in the experiment. The typical threshold current of the device is 30 mA, and the optical output power is about 10 mW at the injection current of 100 mA.

Keywords: sampled grating, complex-coupled, +1st order mode, distributed feedback laser
PACC: 4280S, 7280E, 8115H

1. Introduction

Distributed feedback (DFB) lasers have been widely used in modern optical communication systems for their properties of high stability, narrow-linewidth and high output power.[1,2] However, there exist two major limits in conventional index-coupled DFB lasers: the insufficient threshold gain difference between main and side modes, and the nonuniform axial photon distribution that causes the spatial hole burning.[3−5] Theoretically, pure gain-coupled lasers show large threshold gain difference between main and side modes,[6] higher stability due to the standing wave effect,[7,8] and less spatial hole burning.[9] However, it is difficult to fabricate pure gain gratings because gain variation causes carrier density variation, which in turn causes the variation of the index of refraction. Thus, lasers with both index and gain coupling coefficiens are introduced and such complex-coupled lasers have been reported to exhibit excellent performance.[10,11] Even a small amount of gain coupling (5% of index coupling) presented in complex-coupled DFB lasers can significantly improve the threshold gain difference between main and side modes.[6] Sampled grating is a good tool for tailoring the grating structures,[12−14] and it is an effective way to vary the coupling coefficient on a single wafer or even in the axial direction of a waveguide.[12] So it has been used in tunable distributed Bragg reflector lasers,[15,16] tunable DFB lasers,[17,18] optical filters,[19] and complex-coupled DFB lasers.[12]

In this work, the +1st order reflection of the sampled grating is utilized for single mode operation in a complex-coupled DFB laser. Using sampled grating rather than uniform grating, we can change the lasing wavelength by changing the superperiod of the sampled grating. This method, combined with the double-exposure technique to form the sampled grating, will make it easy to fabricate the multi-wavelength laser array (MLA) by changing the superperiod among stripes on a single wafer instead of using expensive and time-consuming holographic electron beam lithography.

2. Device design

The sampled grating needs to be fabricated on a complex-coupled waveguide structure. It should be

*Project supported by the National High-Tech Research and Development Programm of China (Grant Nos 2006AA01Z256, 2007AA03Z419 and 2007AA03Z417), the National Key Basic Research Programm of China (Grant Nos 2006CB604901 and 2006CB604902), and the National Natural Science Foundation of China (Grant Nos 90401025, 60736036, 60706009 and 60777021).
†E-mail: whuan21@semi.ac.cn

noted that the grating is a building block of the sampled grating and the superperiod Z of the sampled grating can be calculated by

$$\lambda_0 = 2n_{\text{eff}}\Lambda, \tag{1}$$

$$Z = \frac{\lambda_0^2}{2n_{\text{eff}}(\lambda_{+1} - \lambda_0)}, \tag{2}$$

where λ_0 is the Bragg wavelength, $\lambda_{+1}$is the +1st order wavelength of the sampled grating, n_{eff} is the effective index of the complex-coupled waveguide and Λ is the grating period.

The active material gain curve of the waveguide used in the experiment should be taken into consideration as well to make the laser work at the +1st order mode. The Bragg mode is set at the edge of the gain curve, while the +1st order mode is set at the peak. Thus the lasing at the Bragg mode could be suppressed by this design, as shown in Fig.1. The peak of the gain curve is at 1.54 μm, with a full width at half maximum (FWHM) of about 30nm. So λ_0 and λ_{+1} are set at 1.52 μm and 1.54 μm, respectively. The effective index n_{eff} of the waveguide is 3.239. Λ and Z are therefore calculated from Eqs.(1) and (2) to be 234.6 nm and 17.83 μm, respectively. The total length of the device is 300 μm, and the duty cycle of the superstructure is designed to be 2/3.

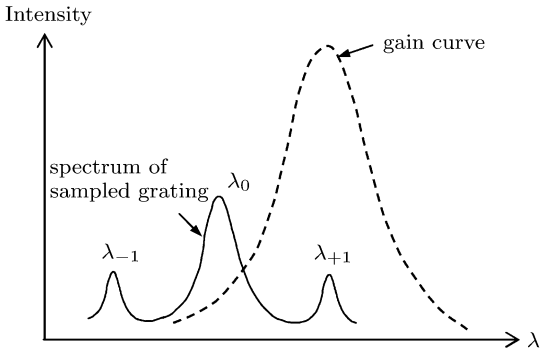


Fig.1. Schematic spectra of the gain curve and the sampled grating.

The transfer matrix method is performed to simulate the designed structure. The calculated model[20] is

$$\begin{pmatrix} E_s^+(z+\Delta z) \\ E_s^-(z+\Delta z) \end{pmatrix} = \begin{pmatrix} \cosh(\gamma\Delta z) - \mathrm{i}\dfrac{\Delta\beta}{\gamma}\sinh(\gamma\Delta z) & -\mathrm{i}\dfrac{\kappa}{\gamma}\sinh(\gamma\Delta z)\mathrm{e}^{-\mathrm{i}\varphi} \\ \mathrm{i}\dfrac{\kappa}{\gamma}\sinh(\gamma\Delta z)\mathrm{e}^{\mathrm{i}\varphi} & \cosh(\gamma\Delta z) + \mathrm{i}\dfrac{\Delta\beta}{\gamma}\sinh(\gamma\Delta z) \end{pmatrix} \begin{pmatrix} E_s^+(z) \\ E_s^-(z) \end{pmatrix}, \tag{3}$$

where E_s^+ and E_s^- are the amplitudes of the forward and backward propagating waves, respectively; φ is the phase of the grating at z, Δz is the longitudinal differential distance, κ is the coupling coefficient and defined as

$$\kappa \equiv \Delta n(\pi/\lambda_0), \tag{4}$$

$$\Delta\beta = \mathrm{i}g/2 + n_{\text{eff}}(2\pi/\lambda_0) - \pi/\Lambda, \tag{5}$$

$$\gamma^2 \equiv \kappa^2 - (\Delta\beta)^2, \tag{6}$$

where g is the intrinsic gain. There are about sixteen superperiods in the device, all of which are assumed to be uniform in the calculation and therefore the parameters are constant. Each superperiod consists of a grating area ($\Delta n = 0.001$) and a non-grating area ($\Delta n = 0$). Figure 2 shows the calculated transmission spectrum of the sampled grating structure.

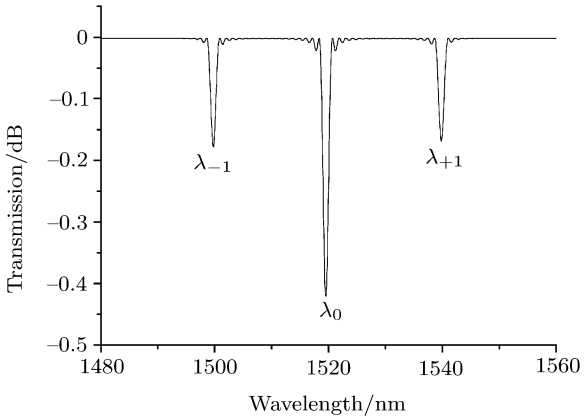


Fig.2. Calculated transmission spectrum of the designed sampled grating.

3. Device fabrication

The device is fabricated by a conventional two-stage metal organic vapour phase epitaxy. Figure 3 shows the schematic structure of the device. An InP buffer layer, a lower optical confinement layer (λ_{PL} = 1200 nm), a MQW active structure ($\lambda_{\mathrm{PL\text{-}MQW}}$ = 1540 nm), an upper optical confinement layer (λ_{PL} = 1200 nm) and a 7 nm-thick n-InP layer are successively grown on a n-InP (100) substrate in the first epitaxial growth. The MQW structure contains five undoped 8 nm-thick 0.7% compressive strain InGaAsP quantum wells. The sampled grating is then formed on the wafer by the double-exposure technique. A conventional holographic exposure is applied to form the configuration of the base grating on the photoresist spread on the wafer. Then a conventional photolithography is used to form the configuration of the sampled grating. After the double exposures, the formation of the sampled grating is completed by etching the n-InP layer and the upper optical confinement layer. For the fabricated devices, the presence of the n-InP layer will modulate the injection current and induce a weak gain coupling to the DFB structure, shown in the inset of Fig.3.

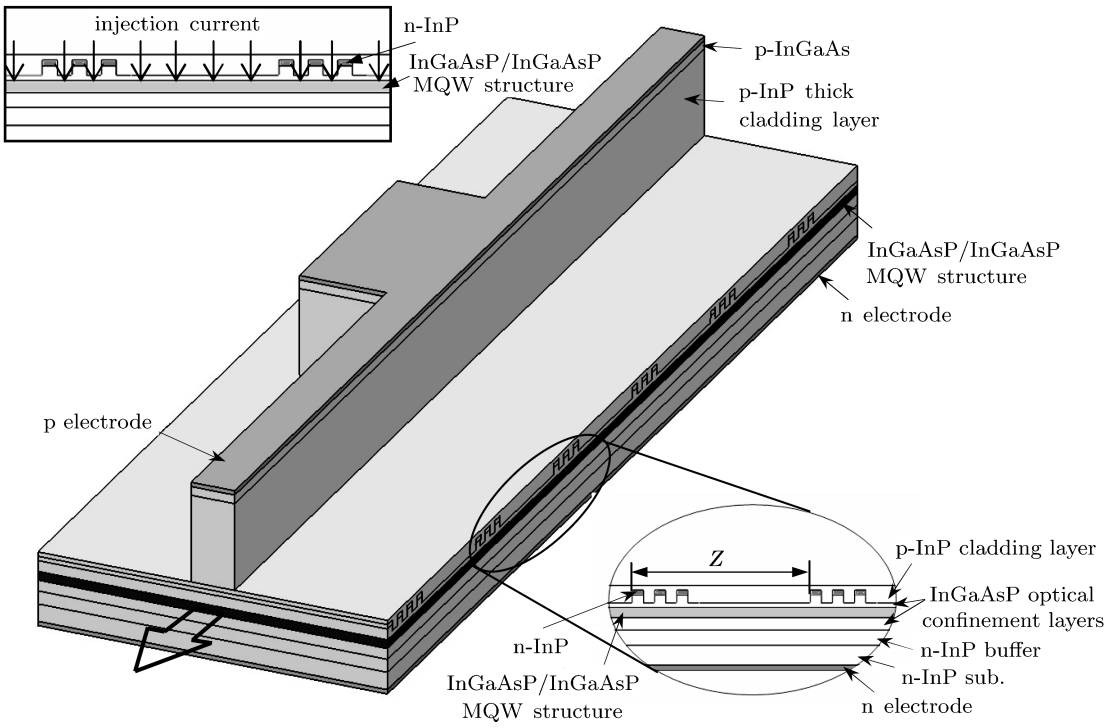


Fig.3. Schematic structure of the designed device. The inset illustrates the modulation of the injection current by the complex-coupled sampled grating.

The Scanning electron microscope (SEM) photograph of the sampled grating is shown in Fig.4. A p-InP cladding layer and a p^+-InGaAs contact layer are successively grown over the entire structure in the second epitaxial growth after the fabrication of the sampled grating. Then conventional ridge waveguide processing is performed. Ti–Au patterned p-contacts and AuGeNi n-contacts are formed on the p-side and the n-side of the device, respectively.

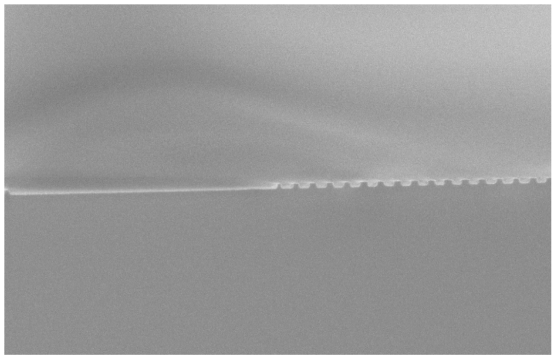


Fig.4. SEM photograph of the sampled grating.

4. Device performance

Figure 5 shows the typical power (P)–current (I) characteristic of the device at room temperature (RT). The continuous wave threshold current of the device is 30 mA at RT. The output power is about 10mW at the injection current of 100mA, and the slope efficiency is about 0.13W·A^{-1}. Figure 6 shows the measured emission spectra of the device at different injection currents at RT. The stopband width is measured to be 1.78 nm in the amplified spontaneous emission spectra, as shown at the bottom of Fig.6. The index-coupling coefficient κ_{i} is calculated to be 47 cm^{-1} from the stopband width. The gain-coupling coefficient κ_{g} can then be estimated to be 18 cm^{-1} in the complex-coupled waveguide. The lasing wavelength is 1.5387 μm at the injection current of 40 mA, and a side mode suppression ratio up to 46dB is achieved, as shown at the top of Fig.6. The lasing wavelength coincides with the designed +1st order mode of the sampled grating, which demonstrates the effectiveness of the design. The dual-peak spectrum of the +1st order mode caused by the hole-burning effect does not appear as the injection current increases. This reveals that the complex-coupled structure can restrain the hole-burning effect, which is one of the main limits in the index-coupled structure.

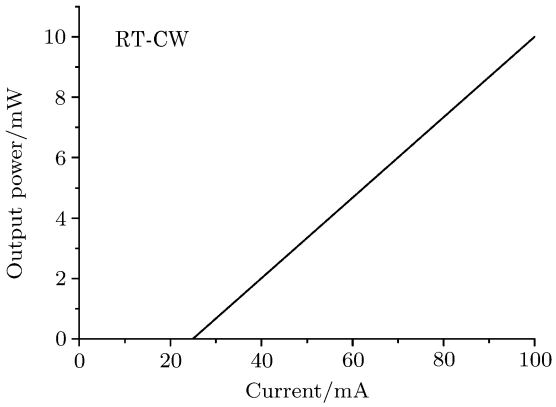


Fig.5. Typical P–I characteristic of the device at room temperature.

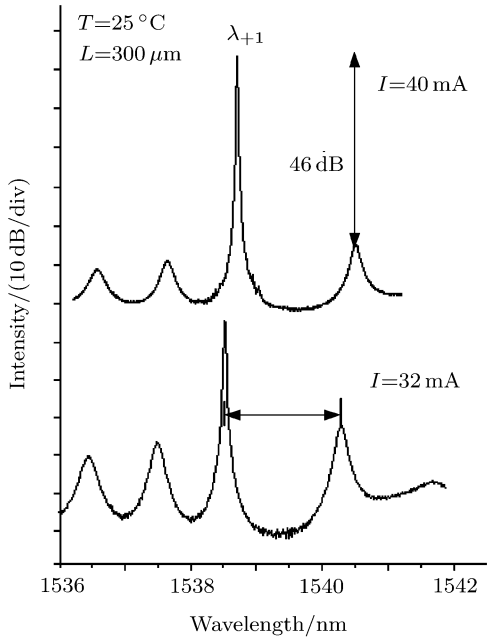


Fig.6. Measured emission spectra of the complex-coupled DFB laser with the sampled grating at different injection currents. The width of the stopband is indicated by the horizontal arrowed line.

It should be noted that the lasing at the Bragg mode has also been observed in some devices which are cleaved from the edge of the wafer. The wafer is not uniform and has a blue shift of the gain curve at the edge of it. The shift makes the Bragg mode closer to the peak of the gain curve and decreases the threshold gain difference between the +1st order and Bragg modes, and in turn causes these two modes to be lasing simultaneously. The lasing intensity of the Bragg mode even exceeds the +1st mode in some devices cleaved from the edge of the wafer, as shown in Fig.7. The presence of Bragg mode can be avoided by shifting it out of the gain curve of the wafer. The lasing wavelength of the +1st order mode as well as the Bragg mode have some differences from the designed values, which are introduced during the fabrication of the sampled grating.

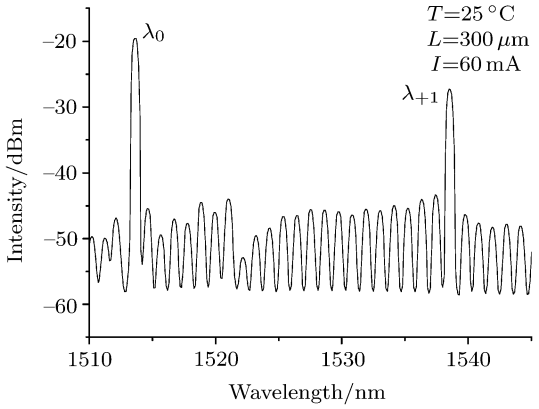


Fig.7. Measured emission spectra of the two laser mode in the devices cleaved from the edge of the wafer.

5. Conclusion

A complex-coupled DFB laser with sampled grating has been designed and fabricated. The sampled

grating can be formed by the double-exposure technique. The +1st order reflection of the sampled grating is chosen to be the lasing wavelength, which is measured to be 1.5387 μm in the experiment. The typical threshold current of the device is 30 mA, and the output power is about 10mW at the injection current of 100 mA. The method in this work could realize different lasing wavelengths among stripes on a single wafer by changing the superperiod Z. Thus the MLA can be fabricated by the method.

Acknowledgments

The authors would like to thank Wang Bao-Jun, Zhou Fan, Pan Jiao-Qing, Shu Hui-Yun for their experimental help, and Wang Lu-Feng, Bian Jing, An Xin for their support on the device test.

References

[1] Wang L, Wang W, Xie H Y, Zhao L J and Zhu H L 2007 *Chin. Phys.* **16** 1459
[2] Zhao Q, Pan J Q, Zhang J, Li B X, Zhou F, Wang B J, Wang L F, Bian J, Zhang L J and Wang W 2006 *Acta Phys. Sin.* **55** 2982 (in Chinese)
[3] Soda H, Ishikawa H and Imai H 1986 *Electron. Lett.* **22** 1047
[4] Ketelsen L, Hoshino I and Ackerman D 1991 *IEEE J. Quantum Electron.* **27** 957
[5] Gu W Y, Shen D X and Xu D X 1999 *Chin. Phys.* **8** 521
[6] Morthier G, Vankwikelberge P, David K and Baets R 1990 *IEEE Photon. Technol. Lett.* **2** 170
[7] Kogelnik H and Shank C V 1972 *J. Appl. Phys.* **43** 2327
[8] David K, Buus J and Baets R G 1992 *IEEE J. Quantum Electron. Lett.* **28** 427
[9] David K, Morthier G, Vankwikelberge P and Baets R 1991 *IEEE J. Quantum Electron.* **27** 1714
[10] Tsang W T, Choa F S, Wu M C, Chen Y K, Logan R A, Sergent A M and Burrus C A 1992 *IEEE Photon.Technol. Lett.* **4** 212
[11] Rast A, Johannes T W and Harth W 1995 *Proc. Inst. Elect. Eng. J. Optoelectron.* **142** 162
[12] Hansmann S, Hillmer H, Walter H, Burkhard H, Hubner B and Kuphal E 1995 *IEEE J. Select. Topics Quantum Electron.* **1** 341
[13] Sang-Bae Kim and Sung-Han Kim 1997 *IEEE Photon. Technol. Lett.* **9** 1078
[14] Chen L H, Fu S H and Song G F 2007 *Acta Phys. Sin.* **56** 1613
[15] Jayaraman V, Mathur A, Coldren L A and Dapkus P D 1993 *IEEE Photon. Technol. Lett.* **5** 489
[16] Suhyun Kim, Youngchul Chul, Su-Hwan Oh and Moon-Ho Park 2004 *IEEE Photon. Technol. Lett.* **16** 15
[17] Hussein M, Vilcot J P and Decoster D 1999 *High Performance Electron Devices for Microwave and Optoelectronic Applications* (London, UK 22-23 Nov. 1999) p215
[18] René Todt T J, Ralf Meyer, Jörg Adler, Reinhard Laroy, Geert Morthier and Markus-Christian Amann 2005 *IEEE Photon. Technol. Lett.* **17** 2514
[19] Shibata Y, Tamamura T, Oku S and Kondo Y 1994 *IEEE Photon. Technol. Lett.* **6** 1222
[20] Lauridsen V C, Sondergaard T, Varming P and Povlsen J H 1997 *23rd European Conference on Optical Communications* (Edinburgh, UK:) p39